Investigation of the surface properties and microstructure of TiO_2 sorbents prepared in supercritical CO_2 for the treatment of Sr^{2+} contaminated effluents

Audrey Hertz, Maxime Duchateau, Yves Barre, Anne Julbe

Investigation of the surface properties and microstructure of TiO_2 sorbents prepared in supercritical CO_2 for the treatment of Sr^{2+} contaminated effluents

Audrey Hertz[*1], Maxime Duchateau[1,2 **], Yves Barre[1], Anne Julbe[2]

[1] CEA, DEN, Univ Montpellier, DE2D, SEAD, Laboratoire des Procédés Supercritiques et de Décontamination, Marcoule, F-30207 Bagnols-sur-Cèze, France

[2] Institut Européen des Membranes (UMR 5635 CNRS, ENSCM, UM), Univ Montpellier, CC47, Place Eugène Bataillon, 34095 Montpellier Cedex 5, France

*corresponding author: audrey.hertz@cea.fr
Tel.: +33-(0)4 66 39 79 27
ORCID ID 0000-0002-7316-0166

** New affiliation: CEA, DEN, DANS, DMN, SEMI, Laboratoire de caractérisations Physico-Chimiques des Matériaux Irradiés, Saclay, F-91191 Gif-sur-Yvette, France

ABSTRACT

Nuclear facilities generate contaminated effluents containing radionuclides (such as Cs, Sr, Co…) that need to be removed for human health and environment protection reasons. Inorganic sorbents are attractive candidate materials because of their high thermochemical and radiation stability. Furthermore, their microstructural and surface properties can be adjusted to increase the radionuclide extraction efficiency. In this study, nanostructured sorbents consisting of aggregated TiO_2 nanocrystals with different surface properties and microstructures were prepared in supercritical CO_2 by varying the synthesis temperature. The Sr^{2+} sorption process was characterized by measuring the surface properties and extraction capacity of the samples as a function of pH. In basic effluents, the Sr sorption capacity of these materials is directly linked to their specific surface area and sorption site density

through a classic physisorption mechanism. Sr^{2+} diffusion into the mesopores leads to rapid initial sorption, which is followed by a slower process driven by a proposed multistep mechanism. This mechanism involves the initial adsorption of partially hydrated Sr^{2+} ions up to complete TiO_2 surface coverage, which implies slower Sr ion diffusion due to steric hindrance in small mesopores thus limiting access to additional secondary sites with lower adsorption energies.

Keywords: Supercritical CO_2, mesoporous TiO_2, physisorption, ion diffusion, effluent treatment.

1. Introduction

An attractive approach to reduce the volume of waste produced in nuclear effluent treatment is to transfer the radioelements (Cs, Sr, Co, Ag, U, Pu, Am...) to a solid substrate (IAEA 2002a). The high resistance to radiation and thermochemical stability of inorganic sorbents make them well suited for these applications (IAEA 2002b). The inorganic compound investigated here, titanium dioxide (TiO_2), has a wide range of applications, notably as a pigment dye, sunscreen agent, photocatalyst, and sorbent. Its attractiveness for radionuclide extraction stems from the fact that on its surface, water sorption leads to the formation of hydroxyl (-OH) groups, which are preferential complexation sites for ions in the aqueous phase (Kim et al. 1995; Kasap et al. 2001; Zhijun et al. 2005; Schmidt & Vogelsberger 2009; Zhang et al. 2009). Studies of the sorption properties of TiO_2 materials have shown that their extraction performance can be optimized by carefully controlling their physicochemical characteristics (Klabunde & Mulukutla 2002; Gao et al. 2004; Gülsen & Tel 2005): a large specific surface area is favorable for metal ion extraction and good sorption site accessibility is essential for fast sorption kinetics. Mesoporous powders with a high surface to volume ratio are beneficial because the active sites are easily accessible. Adsorption performance also seems to depend on the organization of the active sites and therefore on the crystalline structure of the sorbent (Ma & Tu 2011). Synthesizing nanostructured anatase TiO_2 with a high surface area and a well-defined mesoporous network would thus be a key advance for sorption-based decontamination processes.

The TiO_2 sorbents investigated here were synthesized using supercritical carbon dioxide (SC-CO_2) as the reaction solvent, which has been shown to offer several advantages for the preparation and processing of inorganic nanostructured materials (nanopowders, thin films, impregnation of catalysts…) (Sanli et al. 2012; Bozbag et al. 2012). The unique diffusion properties and solvent power of SC-CO_2 allow mesoporous anatase powders with a

high specific area to be prepared at low temperatures without any surfactant (Hertz et al. 2017). The density of the CO_2 is known to be a crucial parameter in controlling the particle size and morphology of metal oxides synthesized in SC-CO_2 (Lane & Zimmerman 2019). In this study, TiO_2 particles were synthesized at a fixed pressure (~300 bar) and the effect of the SC-CO_2 temperature was investigated on their size, morphology, microstructure, surface properties, and the nature and density of the sorption sites. The adsorption mechanism and Sr^{2+} extraction efficiency of these materials were then investigated at different pHs and correlated with their microstructure and surface properties. Finally, the Sr sorption properties of the particles (kinetics, isotherms, maximum capacity, distribution coefficient, and thermodynamic sorption constants) were measured under batch conditions at pH 11.

2. Experimental

2.1. Chemicals

The CO_2 was used as received from Air Liquide (99.998% purity; residual water concentration, 3 ppmv). Titanium (IV) isopropoxide (TIP) (Sigma-Aldrich, 97%) was used as the ceramic precursor, with nitric acid (HNO_3) (Sigma-Aldrich, 69 %) as the sol stabilizer and isopropanol (Sigma-Aldrich, 99.9%) as co-solvent. The sorption experiments were performed using deionized water, $NaNO_3$ (Sigma-Aldrich, 99.5%) and $Sr(NO_3)_2$ (Sigma-Aldrich, 99%). Commercial P25 TiO_2 powder (Degussa, Evonik), composed of 80% anatase and 20% rutile, was used as TiO_2 reference for comparison of Sr^{2+} sorption kinetics (SEM photograph in Fig. S1).

2.2. TiO_2 synthesis in supercritical CO_2

TiO_2 powders were synthesized in SC-CO_2 using a batch reactor (described in (Hertz et al. 2017)), consisting of a 0.5 L vessel which can be heated up to 350°C and can withstand

operating pressures up to ~30 MPa. The TIP sol-gel precursor (50 ml of isopropanol + 10 ml of TIP + 5 ml of nitric acid) was poured into the reactor, the reactor was closed and CO_2 was injected up to a pressure of ~5 MPa. The device was then heated (thus increasing the pressure) up to the target temperature (150°C, 250°C, or 350°C) and pressure (30 MPa), which were maintained for 1 h. The TiO_2 powders (#P150 #P250 #P350, prepared at 150°C, 250°C or 350°C, respectively) formed by thermal decomposition of the precursor and were recovered after the reactor was depressurized and returned to room temperature.

2.3. Structural, microstructural and chemical characterizations

The crystalline structure of the TiO_2 powders was investigated by X-ray diffraction (XRD, X'Pert PRO-PANalytical) using Cu Kα radiation. X-ray induced photoelectron spectroscopy (XPS, Thermo Electron ESCALAB 250) was performed under ultra-vacuum (10^{-10} mbar) using a monochromatic aluminum source to identify chemical elements and their bonds at the extreme surface of the particles. Fourier-transform infrared (FTIR) spectra were measured in absorption mode using a Perkin-Elmer Spectrum 100 spectrometer, the thermogravimetric analysis (TGA) and differential scanning calorimetry (DSC) were performed using a Setaram Setsys Evolution 16 device associated with Hiden QGA 300 mass spectrometer. The powders were observed by field-emission scanning electron microscopy (FESEM, Hitachi S4800) and the size, structure and shape of primary particles were evaluated by transmission electron microscopy (TEM, JEOL 2010F). Particle size distributions were determined by SEM image analysis (FEI Inspect S50). Nitrogen adsorption–desorption isotherms were measured using a Micromeritics ASAP 2020 device and specific surface areas, pore volumes and pore sizes were determined using the Brunauer–Emmett–Teller and Barrett–Joyner–Halenda methods. Surface acidity constants (Ka), points of zero charge (PZC) and sorption site densities were determined using potentiometric acid-base titrations, and zeta

potentials were measured by electrophoretic light scattering (Malvern Zetasizer) to determine the isoelectric point (IEP) of the particles. The pKa values associated with the acid constants Ka1 (pKa1, Ti-OH site protonation) and Ka2 (pKa2, Ti-OH site deprotonation) were determined from titration tests with a strong acid (0.1 M HNO_3) under N_2 flow.

2.4. Batch sorption experiments

2.4.1. Sr^{2+} sorption efficiency

Sorption experiments with Sr^{2+} ions were performed in batch mode at ambient temperature (25°C). Samples (10 mg) of TiO_2 powder were suspended in closed flasks containing aqueous Sr^{2+} solutions with N_2 bubbling to avoid any precipitation of strontium through the formation of carbonate species with CO_2. The suspensions were stirred, collected at fixed times and filtered. The filtrates were analyzed by inductively coupled plasma atomic emission spectrometry (ICP-AES, Thermo Scientific iCAP 6000) to quantify the Sr^{2+} concentration. The concentration data were then used to calculate Sr^{2+} sorption capacities: $Q(mg/g) = \frac{(C_0 - C_f) \times V}{C_f \times m}$, and distribution coefficients: $Kd\ (mL/g) = \frac{Q}{C_{eq}}$ where C_0, C_f and C_{eq} (mg/L) are the initial, final and equilibrium Sr^{2+} concentrations, and m (g) and V (L) are the TiO_2 mass and the volume of the suspension, respectively.

2.4.2. Sorption kinetics

Kinetic experiments were conducted using 1 L of a 50 mg/L Sr^{2+} solution whose pH was adjusted to ~11 by adding KOH and containing 0.5 g/L sorbent. The Sr^{2+} sorption capacity (Q_t) was plotted versus time to determine the equilibrium time (stabilization of the sorption capacity) and the corresponding value of the sorption capacity (Q_{eq}).

2.4.3. pH isotherms

The effect of pH on the sorption process was evaluated by measuring the Sr^{2+} sorption capacity of suspensions of 0.2 g/L sorbent in 10 mg/L Sr^{2+} solutions whose pH was adjusted to between 2 and 12 by adding either NaOH or HNO_3. Sorption capacities were measured after a contact time of 2 h.

2.4.4. Concentration isotherms

The effect of the Sr^{2+} concentration was assessed by measuring sorption isotherms in 50 mL suspensions of 0.2 g/L of sorbent in solutions, containing up to 120 mg/L of Sr^{2+}. The pH was adjusted to ~11 with KOH and the contact time was 40 h.

3. Results and discussion

3.1. Characteristics of the TiO_2 powders

3.1.1. Morphology and microstructure

The morphology and characteristic parameters of the TiO_2 powders synthesized at 150, 250 and 350°C in SC-CO_2, are compared in Fig. 1 and Table 1. The powders are all composed of spherical micrometric particles (microspheres) containing small aggregates (secondary particles) of nanocrystals (primary particles). The sizes distributions of TiO_2 nanocrystal (determined by TEM), microsphere diameters (SEM) and BJH pore diameters (N_2 physisorption) are shown in Fig. 2.

The microsphere size distributions in Fig. 2a show that there are two distinct populations of particles in the powders. The first is centered at 1.5 µm in all the samples and predominates in #P350, while the second is a broader distribution of larger particles with a maximum at ~5 µm for #P150, ~3 µm for #P250 and ~4 µm for #P350 and is weaker in the latter. The mean diameter of the microspheres is inversely related to the synthesis temperature (3 µm, 2.2 µm and 2 µm for #P150, #P250 and #P350 respectively). Within the microspheres, the secondary

particles (15 to 50 nm) are composed of nanocrystals whose mean size (d(TEM) = 5–18 nm) and size distribution (Fig. 2b) also depend on the synthesis temperature.

As detailed in a previous article (Hertz et al. 2017) the decrease of SC-CO_2 density when temperature increases, and the associated increase of self-diffusion coefficients for nanoparticles and/or reacting species, favor reaction kinetics and crystallite growth. Crystallite growth seems to be heterogeneous at 350ºC, certainly due to multi-step precipitation during the temperature rise step in the reactor (Hertz et al. 2010), yielding a wide (bimodal) particle size distribution for #P350 with maxima at ~15 and 35 nm.

The size distributions in the #P250 and #P150 powders are narrower and centered at 7 and 5 nm, respectively. The largest microspheres (~5 µm) and smallest primary particles (~5 nm) were obtained at the lowest reaction temperature (150°C). This indicates that the primary particles have a strong tendency to aggregate, probably because of both small primary particle size (to minimize surface energy) and presence of species on the surface of the particles that are not all decomposed at this temperature. At 350°C, heterogeneous nanocrystal growth leads to a broader distribution of microsphere sizes. The larger TiO_2 crystals (formed by coalescence of small crystallite stacks) yield the smallest (most compact) microspheres.

Figure 3a show that all three powders consist of anatase TiO_2 (JCPDS card 21-1272). The average size of crystalline mono-domains (d(XRD); Table 1) were estimated by applying the Scherrer formula to the (101) peak, with a shape factor of 0.96 (Oskam et al. 2003). The results are in good agreement with the TEM observations of nanocrystals, with the average size of crystalline mono-domains increasing with the synthesis temperature from 6 to 13 nm.

As expected, the specific surface area, pore volume and pore size distribution of the microspheres also depend on the synthesis temperature (Table 1). The specific surface area of the microspheres is inversely correlated with the synthesis temperature, in keeping with the growth of larger TiO_2 crystallites at higher temperatures. The N_2 physisorption isotherms

(Fig. S2) were of type IV, which is typical of mesoporous materials. The pore size distributions derived from the desorption branch (Fig. 2c) are monomodal for all three samples but the pore size and size distribution increase with the synthesis temperature.

As shown in table 1, the XRD, TEM and N2 physisorption analysis revealed that the measured crystallite sizes (domains) correspond to the primary particles composing the TiO2 microspheres. The whole surface of these primary particles is accessible to N2 molecules. As expected, when the temperature increases, the growth of crystallite causes a drop in the specific surface area.

3.1.2. Functional groups (sorption sites) and adsorbed species

The presence of functional groups (correlated to the density of sorption sites) on the particles has been evidenced by XPS, FTIR and TGA. The main results are presented in Fig. 3 and Tables 2 and 3.

The FTIR spectra (Fig. 3c) of the powders show a band at 426 cm^{-1} from the Ti-O bond in anatase (Vuk et al. 2005) and a broad band in the range 2700–3600 cm^{-1}, typical of adsorbed water and hydroxyl groups (Morterra 1988). Part of the broad band ranging from 2700 to 3600 cm^{-1} can also be assigned to O-H bonds in carboxylic acid (inseparable from those of Ti-OH and H-O-H) as well as the wide band at 1379 cm^{-1}. In the #P150 spectrum, the bands at 1712 and 1687 cm^{-1} correspond to C=O stretching vibrations in saturated and unsaturated carboxylic acid. The band at 1300 cm^{-1} is characteristic for the single C-O bond in carboxylic acids. This functional group is not observed in the powders synthesized at higher temperatures. In addition, the bands observed at 2970, 2930 and 2880 cm^{-1} for #P150 correspond to $-CH_2$ and $-CH_3$ groups from residual isopropanol or TTIP. The intensity of these bands decreases for #P250 and they completely disappear for #P350 sample. The bands observed at 1160, 1128 and 1106 cm^{-1} for #P150 also correspond to isopropanol. We can thus

conclude that an increase of the synthesis temperature facilitates the elimination of both unreacted precursor and isopropanol during reactor depressurization at the end of the synthesis.

The XPS data (Fig. 3b, Table 2) show that all three powders have a high surface carbon content, partly in the form of carboxylic acid groups. The intensity of the C=O band from carbonyl and carboxylic acid groups is inversely related to the synthesis temperature. The small number of C-O (Ti-C-O) bonds observed in all the samples may come from the partial degradation of organic reagents (uncomplete oxidation (Hertz et al. 2017)) during synthesis in SC-CO_2. There is also evidence of surface defects: the O/Ti atomic ratio (Table 2) is slightly higher than 2 (the value expected for anatase TiO_2) in the TiO_2 lattice (indicating the presence of Ti^{3+} instead of Ti^{2+}), while increasing the synthesis temperature leads to a decrease in the proportion of stoichiometric defects such as oxygen vacancies ([TiO_{2-x}] / [TiO_2]) .

Finally, the TGA curves (Fig. 3d-g, Table 3**)** show a first thermal event for all samples at $T <$ 150ºC, which corresponds to the evaporation of physisorbed water. The higher water content of the powders produced at low temperatures is directly related to their higher specific surface area. A second weight loss event, corresponding to the dehydration and dehydrogenation of carboxylic acid, is observed for the #P150 and #P250 samples between 150 and 280°C. The final weight loss between 280°C and 400°C was attributed to the removal of chemically bonded hydroxyl groups and to the complete degradation of carbon species (formed by uncomplete oxidation of isopropanol and TTIP during SC-CO_2 synthesis (Hertz et al. 2017)).

3.1.3. Assessment on TiO_2 microsphere formation

The thermal decomposition of TTIP in CO_2-SC medium leads to the formation of nanostructured TiO_2 anatase microspheres. These spheres are made up of an assembly of

secondary particles, themselves made up of aggregated primary particles (nanocrystals). These primary particles form a mesoporous network developing large specific surface areas. The preparation temperature has no impact on the crystalline structure and morphology of the TiO_2 microspheres, although the size of mesopores decreases when the synthesis temperature decreases. At low temperature, a high specific surface area is measured, due to the small size of primary nanocrystals. These nanocrystals have a large number of defects (vacancies, Ti^{3+} and Ti^{2+} species), and provide high density of surface sorption sites (-OH and -COOH). The powders produced at 150°C contain carboxylic acid groups (-COOH) in addition to the Ti-OH sites. The degradation of -COOH groups for synthesis temperatures beyond 250°C yields residual carbon species (uncompleted oxidation in SC-CO2) on powder surface.

These different phenomena are mainly related to the evolution vs. synthesis temperature in SC-CO_2 of the diffusion and integration rates of the growing units. Microspheres are formed by aggregation/agglomeration of nanocrystals. Small crystal sizes accelerate the aggregation kinetics by promoting attractive colloidal interactions. Thereby, the specific properties of SC-CO_2 (viscosity, diffusion coefficients) which can be modulated by temperature, play a key role in nanocrystals mobility. Indeed, a decrease in temperature lowers the viscosity of SC-CO_2, thus potentially favoring the aggregation kinetics of crystallites and secondary particles. In addition, the carboxylic acid groups on #P150 powder surface might promote the formation of hydrogen bonds through their -OH groups and further accelerate aggregation.

3.2. Surface properties in aqueous media – influence of pH on sorption

The surface properties of the TiO_2 sorbent in aqueous media are important for understanding the ion extraction mechanism in solution. The surface charge resulting from the acid-base equilibrium between water and Ti-OH sites determines whether anions or cations

are adsorbed, while the number of Ti-OH sorption sites can affect the sorption efficiency. The measurements performed of the acid-base properties of the powders (surface charge, PZC, IEP and pKa) and the number of surface sites (pH titration, zeta potential) are presented in Table 4. Figure S3 shows the concentrations of protonated [Ti-OH_2^+] and deprotonated [Ti-O^-] species and the surface charge (σ_0) estimated from titration experiments and Fig. 5a shows the evolution of the surface charge as a function of pH and the PZC of the three samples. The absolute surface charge (in C/g) is inversely related to the synthesis temperature, which can be explained by the decrease in hydroxyl site density and specific surface area as the synthesis temperature is increased. The PZC values of the #P250 and #P350 powders are similar (pH 5.7 ± 0.3 and 6.2 ± 0.3, respectively) while the PZC of the #P150 sample is more acidic because of the presence of carboxylic acid groups (–COOH).

The fact that the IEPs measured for suspensions of the samples in 10^{-2} M $NaNO_3$ solutions (Fig. 4b) are close to the PZC values shows that there is no specific adsorption of Na^+ or NO_3^- ions on the TiO_2 hydroxyl sites. The surface charge of the powders (Fig. 4a) is therefore representative of the density of deprotonated -OH sites (nm^{-2}), which is much higher in the #P150 sample than in the #P250 and #P350 powders, probably because of the additional carboxylic acid groups (-COOH) and greater number of defects (oxygen vacancies, Ti^{3+}), which promote the formation of -OH sites.

Finally, Fig. 4c shows that at pHs < pKa1, the surface sites (predominantly Ti-OH_2^+) are positively charged and tend to repel Sr^{2+} ions. The carboxylic acid groups on the surface of the #P150 particles, which dissociate at a lower pH than the hydroxyl sites, allow a small amount of Sr^{2+} sorption at acidic pHs. At pHs between the PZC and pKa2, the particles are negatively charged overall, but the surface sites are mainly neutral (Ti-OH). At pHs above pKa2, the negatively charged Ti-O^- sites attract Sr^{2+} ions and the extraction capacity is highest at pHs above 10. Since the interactions between the hydroxyl groups (Ti-OH) and Sr^{2+}

ions seem to be purely electrostatic, the adsorption mechanism appears to be outer-sphere complexation.

3.3. Sr^{2+} ion sorption in solutions at pH 11

3.3.1. Sorption kinetics

Figure 5a compares the time evolution of the sorption capacity of the three TiO_2 powders. The corresponding equilibrium capacities and kinetic coefficients were estimated using pseudo-second order modeling (Table 5) (Ho & McKay 1999; Simonin 2016; Inyinbor et al. 2016):

$$\frac{t}{Q_t} = \frac{1}{\mathrm{k} \times Q_{\mathrm{eq}}^2} + \frac{1}{Q_{\mathrm{eq}}} t \qquad (1)$$

where Q_t (mg/g) is the sorption capacity at time t, Q_{eq} (mg/g) is the equilibrium sorption capacity, t is the time in hours and k is the kinetic constant (mg/g/h).

Table 5 also shows the diffusion rate constants Kdiff ($mg/g/h^{1/2}$) determined by fitting the square-root time evolution of the sorption capacities (Fig. 5b), with a Weber-Morris intra-particulate diffusion model (Weber & Morris 1963; Inyinbor et al. 2016):

$$Q(t) = \mathrm{Kdiff} \times \sqrt{t} + \mathrm{constant} \qquad (2)$$

The kinetic curves all show two stages (Fig. 5a,b) with the sorption capacity increasing sharply at first and then more gradually. The data in the second (plateau) stage are well fitted by Eq. (1) but the fits are less accurate for the initial phase. The amounts of Sr retained by the #P350, #P250 and #P150 powders after 5 min contact are respectively 10, 40 and 65 mg/g, which corresponds to ~100% coverage of the adsorption sites (one Sr^{2+} ion adsorbed on two $-O^-$ sites for surface charge compensation). This fast process (Kdiff1 ≈ $400 mg/g/h^{1/2}$) corresponds to a physisorption mechanism without Nernst layer restrictions at the TiO_2 surface. The high specific surface area and sorption site density of the #P150 powder explain why it shows the best Sr^{2+} sorption performance (the highest equilibrium capacity, Q_{eq}

~ 77 mg/g, with fast kinetics: 84% of Q_{eq} in less than 5 min). The diffusion constant for the second, slower process (Kdiff2, Table 5) increases with the size of the mesopores in the samples, which is indicative of intra-particulate/inter-crystallite diffusion limitations. Furthermore, this slower process seems to correspond to the adsorption of more than one Sr^{2+} ion per pair of O^- sites. For #P350 indeed, the slope of the diffusion curve changes twice, once at a capacity corresponding to each Sr^{2+} ion interacting with two $-O^-$ sites and a second time at a capacity corresponding to 1:1 interactions. This suggests that the adsorbed Sr^{2+} ions become hydrated in basic media, leading to the formation of Sr-O^- sites with a lower adsorption energy than the Ti-O^- sites. A surface layer of hydrated Sr^{2+} ions would limit access to additional internal sorption sites and slow down the adsorption kinetics, particularly in the powders with smaller mesopores. These results are therefore consistent with an outer-sphere sorption mechanism.

For comparison, the equilibrium capacity measured for the #P25 commercial TiO_2 powder (S_{BET}~60m^2/g) is around 26 mg/g (Fig. 5a). This capacity is slightly lower than the value measured for #P350 sample (~32 mg/g), in good agreement with its higher specific surface area (90m^2/g). However, the initial sorption kinetic is faster for #P25 (Fig. 5b) due to a better dispersion of its nanocrystals in the suspension (less aggregated particles). This shows that the sorption mechanism for #P25 is not limited by the diffusion of Sr^{2+} ions in the particle mesoporosity, as in the case of TiO_2 microspheres. However, the interest of handling TiO_2 microsphere instead of isolated nanoparticles (health hazard) is still motivating our research activity in this area.

3.3.2. Sr^{2+}sorption isotherms

Figure 6a shows the Sr^{2+} sorption isotherms measured for the three TiO_2 powders. As expected, the #P150 powder has the highest sorption capacity, with a distribution coefficient of ~10^6 mL/g at low Sr^{2+} concentrations (Fig. 6b). This high sorption capacity is explained by the large specific surface area of the #P150 powder. The isotherm profiles do not level out, which is consistent with the proposed multistep adsorption mechanism. The experimental data were fitted using three thermodynamic models (Langmuir, Freundlich and Temkin; Fig. S4), to estimate the maximum sorption capacity (Q_{max}) and the thermodynamic parameters in the models (Table 5) (Dada et al. 2012; Inyinbor et al. 2016; Ajawei et al. 2017).

The Langmuir model describes adsorption in a monolayer with a uniform adsorption site energy and no interactions between vicinal sites. The linearized equation for the Langmuir model is:

$$\frac{1}{Q_{\mathrm{eq}}} = \frac{1}{Q_{\mathrm{max}}} + \frac{1}{K_{\mathrm{L}} \times Q_{\mathrm{max}} \times C_{\mathrm{eq}}} \quad (3)$$

with $$\Delta G = -RT \ln Q_{\mathrm{max}} K_{\mathrm{L}} \quad (4)$$

where Q_{max} (mg/g) is the maximum monolayer coverage capacity, Q_{eq} (mg/g) is the equilibrium sorption capacity, C_{eq} (mg/L) is the equilibrium solution concentration, K_L is the Langmuir isotherm constant (L/mg), and ΔG (KJ/mol) is the sorption free energy, with R, the gas constant and T (K) the temperature.

The Freundlich model describes multilayer adsorption on a heterogeneous surface assuming exponential distributions of active sites and site energies. The linearized equation for the Freundlich model is:

$$\log Q_{eq} = \log K_{\mathrm{F}} + \frac{1}{\mathrm{n}} \log C_{eq} \quad (5)$$

where $1/n$ is the adsorption intensity and K_F is the Freundlich constant (mg/g). When $n = 1$, the partition between the two phases is independent of concentration and the adsorption

isotherm is linear; $n > 1$ corresponds to normal sorption with values from 1 to 10 yielding a favorable isotherm, while $n < 1$ corresponds to cooperative adsorption.

The Temkin model takes into account indirect adsorbate interactions and assumes that the heat of adsorption decreases linearly as surface coverage increases. The linearized equation for the Temkin model is:

$$Q_{\mathrm{eq}} = B \ln A + B \ln C_{\mathrm{eq}} \quad (6)$$

where B is a constant related to the heat of adsorption (ΔH, J/mol) and A is the Temkin isotherm equilibrium binding constant (L/g).

The fitting parameters in all three models provide useful information on the adsorption mechanism. The fact that ΔG in the Langmuir model is negative is consistent with a spontaneous physisorption mechanism, and the inverse relationship between the absolute value of ΔG and the synthesis temperature confirms that #P150 has the most favorable adsorption properties. The values of $1/n$ (~0.2) in the Freundlich model show moreover that the adsorption process is favorable for all the samples. The positive values of the Temkin constant (B) indicate that the adsorption process is endothermic.

In keeping with the proposed complex multi-step physisorption mechanism, the Langmuir model (monolayer adsorption) does not accurately fit the experimental data, and while the fit is improved with the Freundlich equation, these results indicate that adsorption of Sr^{2+} on the TiO_2 sorbents is best described by the Temkin model. This supports the suggested adsorption of several Sr^{2+} ions per active site and the variation of the energy of the adsorption sites with the multi-layered surface coverage. The maximum sorption capacity in the Langmuir model indicates that 1.1–1.6 Sr^{2+} ions per active site on the TiO_2 particles (Table 5), which is higher than expected for a simple electrostatic mechanism (0.5 Sr^{2+} per $–O^-$ or COO- sorption site). The powder with the lowest adsorption site coverage (1.1) is #P150,

probably because of its smaller pores (~4 nm). Since the hydrated diameter of Sr^{2+} ions is ~0.82 nm, steric effects limit the number that can be accommodated in such small pores.

4. Conclusions and prospects

This study shows that TiO_2 powders prepared in SC-CO_2 crystallize as anatase at temperatures as low as 150°C, and that their microstructure and surface properties are favorable for effluent treatment by adsorption. These TiO_2 sorbents are composed of mesoporous micrometric spherical particles formed by the successive agglomeration of primary nanometric TiO_2 particles and particle agglomerates. The mean size of the mesopores increases with the synthesis temperature and this was attributed to the way the primary particles growth and agglomerate. High specific surface areas, up to 275 m^2/g, are obtained at low synthesis temperatures, because of the small crystallites and mesoporous structure (pore diameter ~4 nm) of the particles. Surface hydroxyl and carboxylic acid groups become active adsorption sites in basic media.

The Sr^{2+} extraction properties of these materials depend on the pH of the solution, which affects their surface properties and the overall adsorption mechanism. The specific surface area and number of sorption sites (-OH and -COOH) are the main parameters that affect the adsorption capacity in basic media. Here, the powder prepared at the lowest temperature (150°C) was found to have best adsorption performance, with the mesoporous network providing rapid access (< 5 min) to all surface sorption sites. However, the small size of the mesopores limits further diffusion by steric hindrance due to TiO_2 surface coverage of hydrated Sr^{2+} ions in basic media. This multi-step adsorption mechanism is much more complex than the expected homogeneous physisorption on TiO_2 surface sites and further investigations with complementary experiments such as microcalorimetry are warranted.

Overall though, this study shows that the microstructure and active site density of mesoporous TiO_2 microspheres prepared at 150°C in SC-CO_2 are attractive for adsorption processes, with a high Sr^{2+} sorption capacity in basic media. In addition, the synthesis protocol could be adapted to deposit nanostructured mesoporous films on relevant supports. Work is ongoing on the preparation in SC-CO_2 of hierarchical sorbents with a highly interconnected porous structure by coating mesoporous films on macroporous substrates. The idea is to combine the favorable diffusion properties of the macroporous network with the large active surface area of the nanostructured mesoporous TiO_2. These sorbents could thus be implemented in either column or filtration processes for effective effluent treatment.

Conflict of Interest:

The authors declare that they have no conflict of interest.

Acknowledgements

The authors thank Dr. Martin Drobek and Didier Cot from the IEM for performing respectively the XRD measurements and FESEM observations, and Valérie Flaud from the Institut Charles Gerhardt at the University of Montpellier for the XPS analysis. The authors also thank Adrien Gerenton, Myriam Dunand (SEAD, CEA Marcoule) and Cyrielle Rey (ICSM) for carrying out the N_2 physisorption, ICP analyses and MS-TGA, respectively.

References

IAEA: Management of low and intermediate level radioactive wastes with regard to their chemical toxicity. TECODOC n°1325, Vienna (2002)

IAEA: Application of ion exchange processes for treatment of radioactive waste and management of spent ion exchangers. Technical Report Series n°408 (2002)

Schmidt, J., Vogelsberger, W.: Aqueous long-term solubility of titania nanoparticles and titanium (IV) hydrolysis in a sodium chloride system studied by adsorptive stripping voltammetry. J. Solution Chem. **38**, 1267–1282 (2009)

Zhijun, G., Lijun, N., Zuyi, T.: Sorption of Th (IV) ions onto TiO_2: Effects of contact time, ionic strength, thorium concentration and phosphate. J. Radioanal. Nucl. Chem. **266**, 333–338 (2005)

Zhang, L., Liu, N., Yang, L., Lin, Q.: Sorption behavior of nano-TiO_2 for the removal of selenium ions from aqueous solution. J. Hazard. Mater. **170**, 1197–1203 (2009)

Kasap, S., Tel, H., Piskin, S.: Isotherm, thermodynamic and kinetic studies of Sr^{2+} adsorption on spherical TiO_2/PAN composites. J. Radioanal. Nucl. Chem. **289**, 537–544 (2011)

Kim, K.R., Lee, K.J., Bae, J.H.: Characteristics of cobalt adsorption on prepared TiO_2 and Fe-Ti-O adsorbents in high temperature water. Sep. Sci. Technol. **30**, 963–979 (1995)

Klabunde, K.J., Mulukutla, R.S.: Chemical and catalytic aspects of nanocrystals. Nanoscale Materials in Chemistry, 223–259 (2001).

Gao, Y., Wahi, R., Kan, A.T., Falkner, J.C., Colvin, V.L., Tomson, M.B.: Adsorption of cadmium on anatase nanoparticles effect of crystal size and pH. Langmuir **20**, 9585–9593 (2004)

Gülsen, G., Tel, H.: Preparation of TiO_2–SiO_2 mixed gel spheres for strontium adsorption. J. Hazard. Mater. **120**, 135–142 (2005)

Ma, L., Tu, S.X.: Removal of arsenic from aqueous solution by two types of nano TiO_2 crystals. Environmental Chemistry Letters **9**(4), 465-472 (2011).

Sanli, D., Bozbag, S.E., Erkey, C.: Synthesis of nanostructured materials using supercritical CO_2: Part I. Physical transformations. J. Mater. Sci. **47**, 2995–3025 (2012)

Bozbag, S.E., Sanli, D., Erkey, C.: Synthesis of nanostructured materials using supercritical CO_2: Part II. Chemical transformations. J. Mater. Sci. **47**, 3469–3492 (2012)

Hertz, A., Drobek, M., Ruiz, J.C., Charton, F., Sarrade, S., Guizard, C., Julbe, A.: A detailed insight into the preparation of nanocrystalline TiO_2 powders in supercritical carbon dioxide. J. Mater. Sci. **52**, 12635–12652 (2017)

Lane, M.K.M., Zimmerman, J.: Controlling metal oxide nanoparticle size and shape with supercritical fluid synthesis. Green Chem. **21** 3769–3781 (2019)

Oskam, G., Nellore, A., Penn, R.L., Searson, P.C.: The growth kinetics of TiO_2 nanoparticles from titanium (IV) alkoxide at high water/titanium ratio. J. Phys. Chem. B, **107**, 1734–1738 (2003)

Han, E., K. Vijayarangamuthu, K., Youn, J-S., Y-K. Park, Y-K., S-C. Jung, S-C., Jeon, K-J.,: Degussa P25 TiO_2 modified with H_2O_2 under microwave treatment to enhance photocatalytic properties. Catalysis Today, **303**, 305-312 (2018)

Rui Z.,, Wu, S., Peng, C., Ji, H.: Comparison of TiO_2 Degussa P25 with anatase and rutile crystalline phases for methane combustion Chemical Engineering Journal, **243**, 254-264 (2014)

Morterra, C.: An infrared spectroscopic study of anatase properties. Part 6.—Surface hydration and strong Lewis acidity of pure and sulphate-doped preparations. J. Chem. Soc. Faraday Trans. 1 **84**, 1617–1637 (1988)

Vuk, A.Š., Ješe, R., Orel, B., Dražc, G.: The effect of surface hydroxyl groups on the adsorption properties of nanocrystalline TiO_2 films. Int. J. Photoenergy **7**, 163–168 (2005)

Hertz, A., Corre, Y-M., Sarrade, S., Guizard, C, Julbe, A, Ruiz, J-C., Fournel, B. : Yttria stabilized zirconia synthesis in supercritical CO2: Understanding of particle formation mechanisms in CO_2/co-solvent systems. J. Eur. Ceram. Soc. **30**, 1691-1698 (2010)

Ho, Y.S., McKay, G.: Pseudo-second order model for sorption processes. Process Biochem. **34**, 451–465 (1999)

Simonin, J.P.: On the comparison of pseudo-first order and pseudo-second order rate laws in the modeling of adsorption kinetics. Chem. Eng. J. **300**, 254–263 (2016)

Inyinbor, A.A., Adekola, F.A., Olatunji, G.A. Kinetics, isotherms and thermodynamic modeling of liquid phase adsorption of Rhodamine B dye onto Raphia hookerie fruit epicarp. Water Resour. Ind. **15**, 14–27 (2016)

Weber, W.J., Morris, J.C. Kinetics of adsorption on carbon from solution. J. Sanit. Eng. Div. **89**, 31–60 (1963)

Dada, A.O., Olalekan, A.P., Olatunya, A.M., Dada, O. Langmuir, Freundlich, Temkin and Dubinin–Radushkevich isotherms studies of equilibrium sorption of Zn^{2+} unto phosphoric acid modified rice husk. IOSR J. Appl. Chem. **3**, 38-45 (2012)

Ayawei, N., Ebelegi, A.N., Wankasi, D. Modelling and interpretation of adsorption isotherms. J. Chem. 3039817 (2017).

Captions

Table 1 Morphological and microstructural characteristics of TiO_2 microspheres prepared in supercritical CO_2 at 150, 250 and 350ºC, in comparison with a P25 commercial TiO_2 powder provided by Degussa-Evonik (literature data (Rui et al. 2014, Han et al. 2018))

Table 2 Semi-quantitative XPS analyzes of C/Ti and O/Ti atomic ratios and the proportion of bonds (at. %) involving oxygen (O1s) in TiO_2 microspheres prepared in supercritical CO_2 at 150, 250 and 350ºC

Table 3 Thermogravimetric analysis of TiO_2 microspheres prepared in supercritical CO_2 at 150, 250 and 350ºC

Table 4 Surface properties of TiO_2 microspheres prepared in supercritical CO_2 at 150, 250 and 350ºC estimated by acid-base titration and zeta-potentiometry

Table 5 Kinetic and isotherm modeling data for suspensions of TiO_2 microspheres prepared in supercritical CO_2 at 150, 250 and 350ºC

Table 1 Morphological and microstructural characteristics of TiO_2 microspheres prepared in supercritical CO_2 at 150, 250 and 350ºC, in comparison with a P25 commercial TiO_2 powder provided by Degussa-Evonik (literature data (Rui et al. 2014, Han et al. 2018))

Powder	Size of rystalline mono-domains / nanocrystals[a] (nm)	Microsphere diameters (µm)		S_{BET}[b] (m^2/g)	Pore volume (cm^3/g)	d_{BJH}[c] (nm)
		Average	Max of the distribution			
#P150	6, 6, 5	3	1.5 & 5	275	0.37	4
#P250	8, 7, 8	2.5	1.5 & 3	190	0.55	7
#P350	16, 13, 18	2	1.5 & 4	95	0.45	14
#P25 (Rui et al. 2014, Han et al. 2018)	21	15-40nm slightly agglomerated (SEM/TEM primary particles)		55-65	0.17-0.22	12-18

[a]The three values correspond to measurements by N_2 adsorption, X-ray diffraction and transmission electron microscopy

[b]Specific surface area determined using the BET method

[c]Average pore size determined using the BJH method

Table 2 Semi-quantitative XPS analyzes of C/Ti and O/Ti atomic ratios and the proportion of bonds (at. %) involving oxygen (O1s) in TiO_2 microspheres prepared in supercritical CO_2 at 150, 250 and 350ºC

Powder	C1s	O1s	Ti2p3	O/Ti	C/Ti	TiO_{2-x}	TiO_2	O=C/O-H	O-C
#P150	38	45	17	2.7	2.2	11	60	21	7
#P250	39	43	17.1	2.5	2.3	9	69	15	7
#P350	40	42	18	2.3	2.2	3	77	11	8

All values in atomic percent

Table 3 Thermogravimetric analysis of TiO_2 microspheres prepared in supercritical CO_2 at 150, 250 and 350ºC

Temperature range	< 150 ºC	150–280 ºC	> 280 ºC	25–500 ºC
Powder	Δm_1 (%)	Δm_2 (%)	Δm_3 (%)	Total Δm (%)
#P150	4.8	4.1	7.1	16.0
#P250	2.5	1	5.1	8.6
#P350	1.4	-	2.3	3.7
Volatilized species[a]	Physisorbed water	Degradation of unreacted precursors and -COOH dehydration and dehydrogenation	Degradation of structural water -OH and residual –COOH	

[a]Identified by mass spectrometry

Table 4 Surface properties of TiO_2 microspheres prepared in supercritical CO_2 at 150, 250 and 350ºC estimated by acid-base titration and zeta-potentiometry

Powder	pKa1	pKa2	PZC	IEP	Deprotonated sites (nm^{-2})
#P150	4.7	8	4.2	4.7	3.4
#P250	5.0	7.8	5.7	5.9	2
#P350	5.1	7.8	6.2	6.1	1.9

PZC, point of zero charge; IEP, isoelectric point

Table 5 Kinetic and isotherm modeling data for suspensions of TiO_2 microspheres prepared in supercritical CO_2 at 150, 250 and 350ºC

		#P150	#P250	#P350
Kinetic data				
Q_{eq} (mg/g) - Pseudo 2nd order		77.5	47.4	32.4
Kreaction 2nd order (mg/g/h)		0.083	0.065	0.053
Kdiff 1 (mg/g/$h^{1/2}$)		~400	~400	~400
Kdiff 2 (mg/g/$h^{1/2}$)		6.7	8.0	16.4
Kdiff 3 (mg/g/$h^{1/2}$)		1.7	1.2	4.6
Q (mg/g) at the end of first sorption step (5min)		65	40	10
Sr adsorbed in 5 min (% of Q_{eq})		84%	86%	30%
Number of Sr atom /site at the end of first sorption step (5min)		0.5	0.7	0.4
Number of Sr atom /site at the end of second sorption step		0.5	0.8	1
Isotherm data				
Langmuir model Equation (3)	slope = 1 / Q_{max}	0.0068	0.0111	0.0283
	intercept = 1 / (Q_{max}* L)	0.0062	0.017	0.0325
	Q_{max} (mg/g)	147	90	35
	K_L (L/mg)	1.1	0.7	0.9
	ΔG (KJ/mol)	-12.6	-10.1	-8.5
	Correlation coefficient	**0.982**	**0.961**	**0.951**
Freundlich model Equation (5)	slope = 1 / n	0.2115	0.1484	0.2066
	intercept = log K	1.8641	1.6952	1.1967
	n	4.7	6.7	4.8
	K_F (mg/g)	73	50	16
	Correlation coefficient	**0.982**	**0.980**	**0.985**
Temkin model Equation (6)	slope = B	15.525	8.2042	3.6155
	intercept = B ln$A$	84.546	53.463	19.127
	B (J/mol)	15.5	8.2	3.6
	A (L/g)	232	676	198
	Correlation coefficient	**0.993**	**0.994**	**0.981**
Density of Sr atoms at Q_{max} (nm^{-2})		3.7	3.2	2.6
Number of Sr atoms per adsorption site at Q_{max}		1.1	1.6	1.4

Captions

Figure 1 (a–j) Scanning and transmission electron micrographs of TiO_2 microspheres prepared in supercritical CO_2 at (a, b, c, d) 150ºC, (e, f, g) 250ºC and (h, i, j) 350ºC. (k) Schematic representation of the microstructure of the TiO_2 particles

Figure 2 Distributions of (a) crystallite sizes determined by transmission electron microscopy, (b) microsphere diameters determined by scanning electron microscopy and (c) pore sizes determined using the Barrett–Joyner–Halenda method for TiO_2 microspheres prepared in supercritical CO_2 at 150, 250 and 350ºC

Figure 3 (a) X-ray diffraction patterns of TiO_2 microspheres prepared in supercritical CO_2 at 150, 250 and 350ºC; (b) O1s X-ray photoelectron spectrum of the powder prepared at 250ºC; (c) FTIR spectra with expanded view in the ranges 900-1800 cm^{-1} and 2400-3600 cm^{-1} for #P150, #P250 and #P350 powders; (d) heat flow and amounts of H_2O and CO_2 released as a function of temperature for #P150 sample; and (e–g) thermogravimetric curves for the powders prepared at (e) 150ºC, (f) 250ºC and (g) 350ºC.

Figure 4 Evolution of (a) the surface charge, (b) the zeta potential (0.3 g/l TiO_2; 10^{-2} M $NaNO_3$) and (c) Sr^{2+} sorption capacity after 3 h contact time as a function of the pH of the solution, for suspensions of TiO_2 microspheres prepared in supercritical CO_2 at 150, 250 and 350ºC

Figure 5 (a) Kinetic curves measured for suspensions of TiO_2 microspheres prepared in supercritical CO_2 at 150, 250 and 350ºC and commercial P25 TiO_2 (1 L, 50ppm Sr^{2+}, 0.5g/L

sorbent, pH 11) with second order kinetic fittings, and (b) Weber-Morris intra-particulate diffusion modeling of the same data

Figure 6 (a) Concentration adsorption isotherms fitted with the Temkin equation, (b) distribution (K_d) isotherms for TiO_2 microspheres prepared in supercritical CO_2 at 150, 250 and 350ºC in suspensions at pH 11

Figure 1 (a–j) Scanning and transmission electron micrographs of TiO_2 microspheres prepared in supercritical CO_2 at (a, b, c, d) 150ºC, (e, f, g) 250ºC and (h, i, j) 350ºC. (k) Schematic representation of the microstructure of the TiO_2 particles

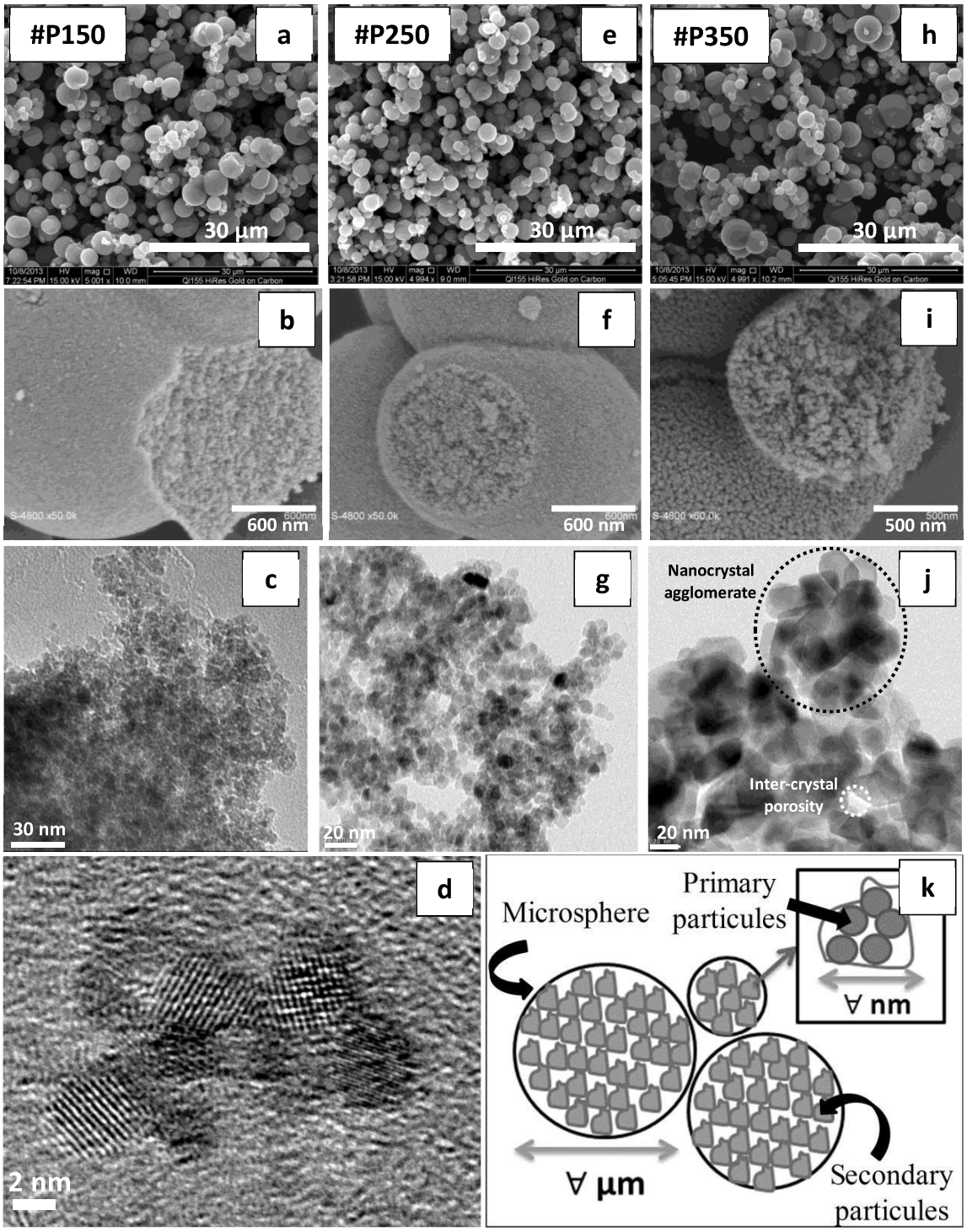

Figure 2 Distributions of (a) nanocrystals diameter determined by transmission electron microscopy, (b) microsphere diameters determined by scanning electron microscopy and (c) pore sizes determined using the Barrett–Joyner–Halenda method for TiO_2 microspheres prepared in supercritical CO_2 at 150, 250 and 350ºC

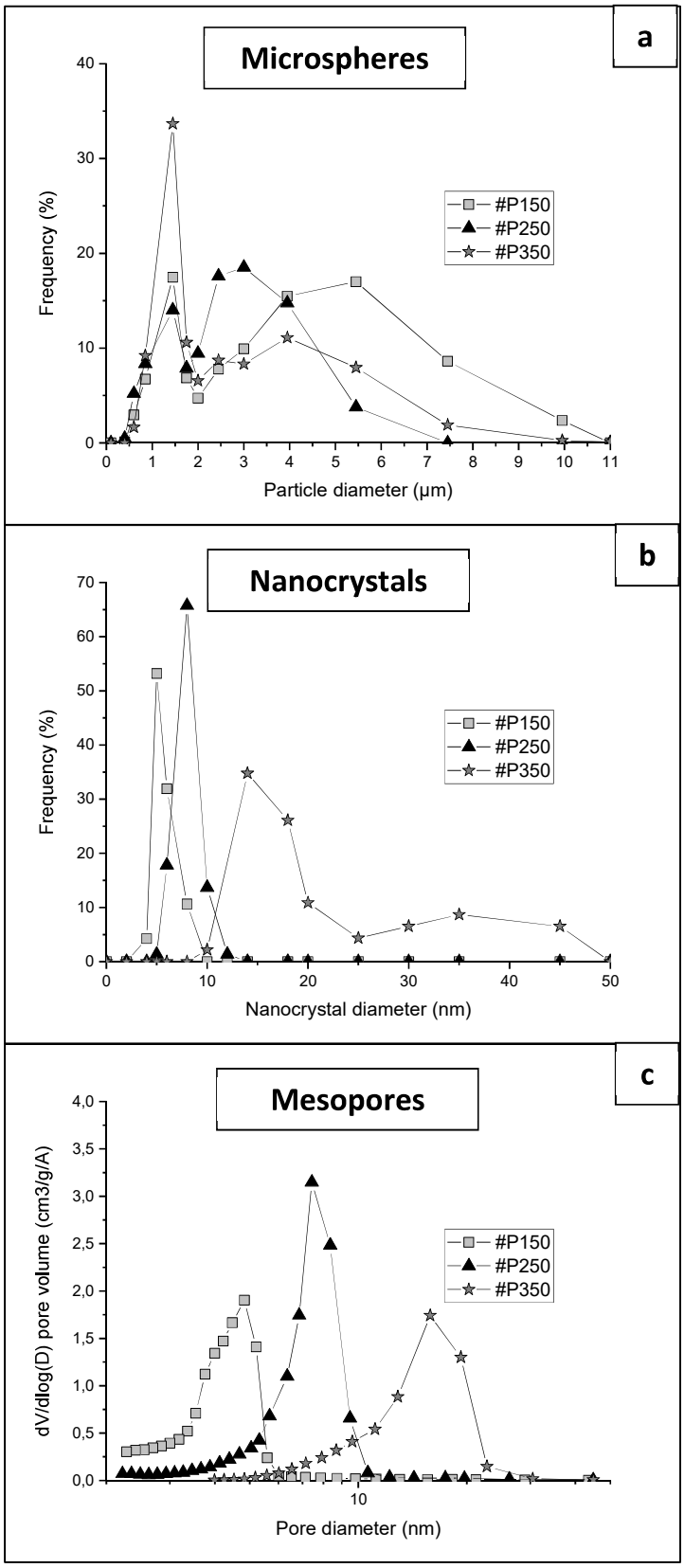

Figure 3 (a) X-ray diffraction patterns of TiO_2 microspheres prepared in supercritical CO_2 at 150, 250 and 350ºC; (b) O1s X-ray photoelectron spectrum of the powder prepared at 250ºC; (c) FTIR spectra with expanded view in the ranges 900-1800 cm^{-1} and 2400-3600 cm^{-1} for #P150, #P250 and #P350 powders; (d) heat flow and amounts of H_2O and CO_2 released as a function of temperature for #P150 sample; and (e–g) thermogravimetric curves for the powders prepared at (e) 150ºC, (f) 250ºC and (g) 350ºC.

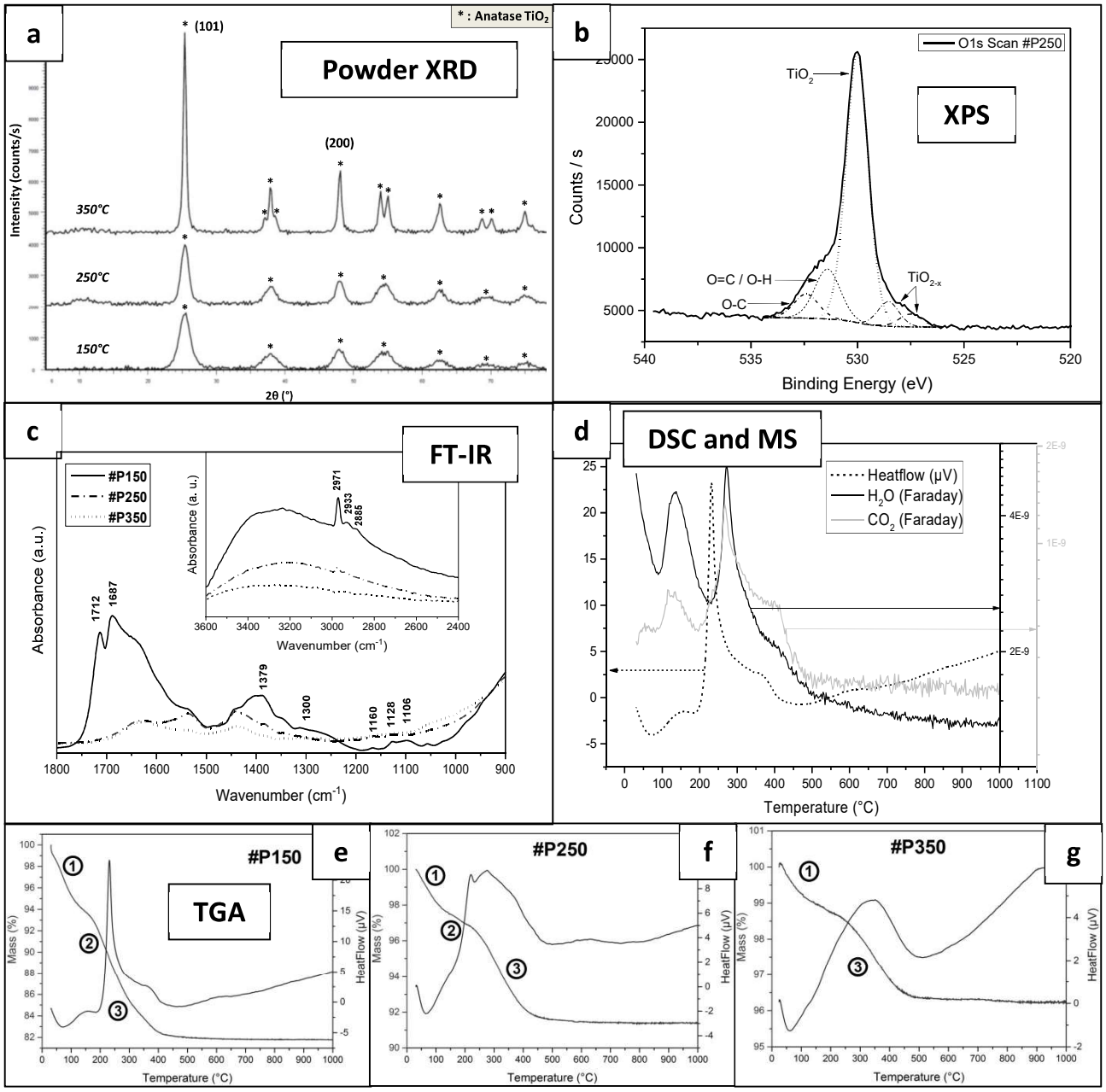

Figure 4 Evolution of (a) the surface charge, (b) the zeta potential (0.3 g/l TiO_2; 10^{-2} M $NaNO_3$) and (c) Sr^{2+} sorption capacity after 3 h contact time as a function of the pH of the solution, for suspensions of TiO_2 microspheres prepared in supercritical CO_2 at 150, 250 and 350ºC

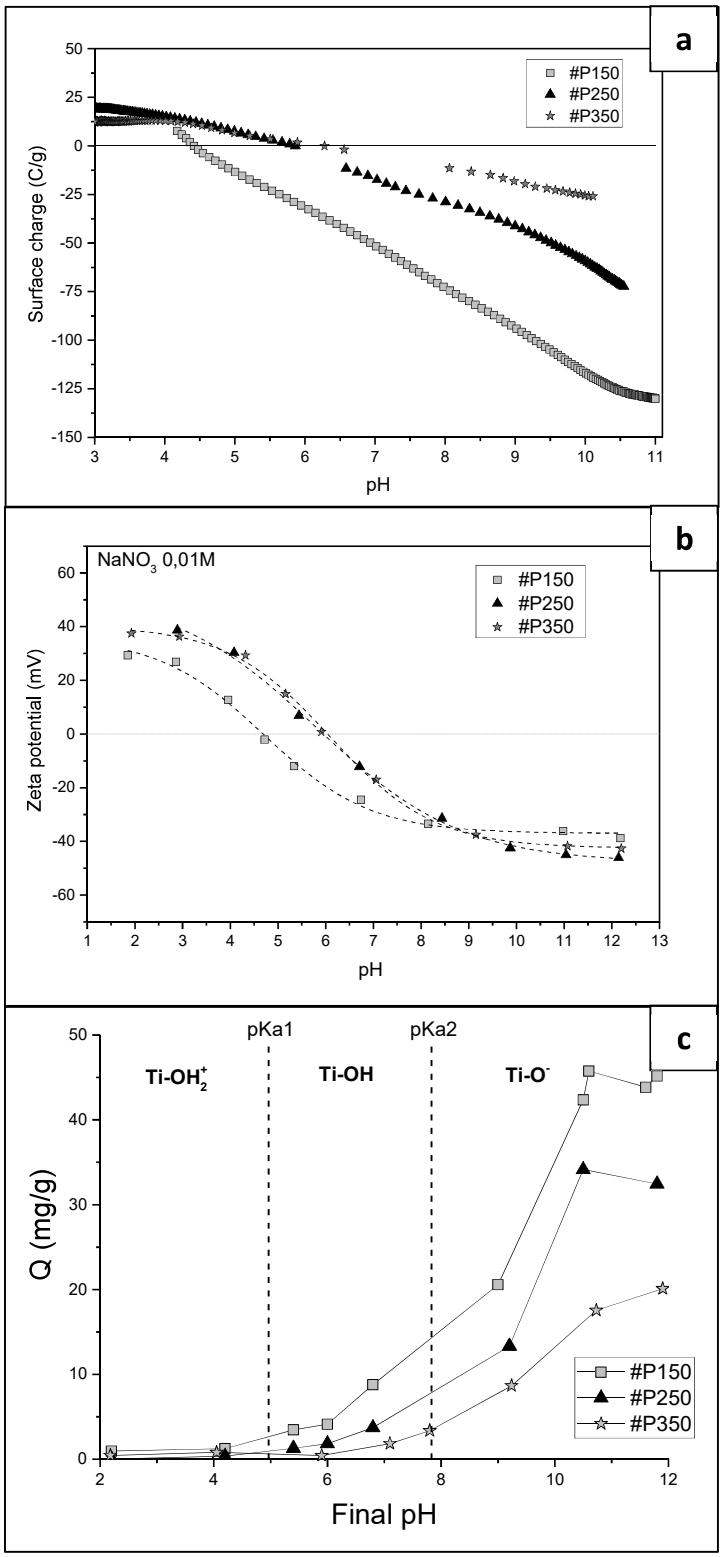

Figure 5 (a) Kinetic curves measured for suspensions of TiO_2 microspheres prepared in supercritical CO_2 at 150, 250 and 350ºC and commercial P25 TiO_2 (1 L, 50ppm Sr^{2+}, 0.5g/L sorbent, pH 11) with second order kinetic fittings, and (b) Weber-Morris intra-particulate diffusion modeling of the same data.

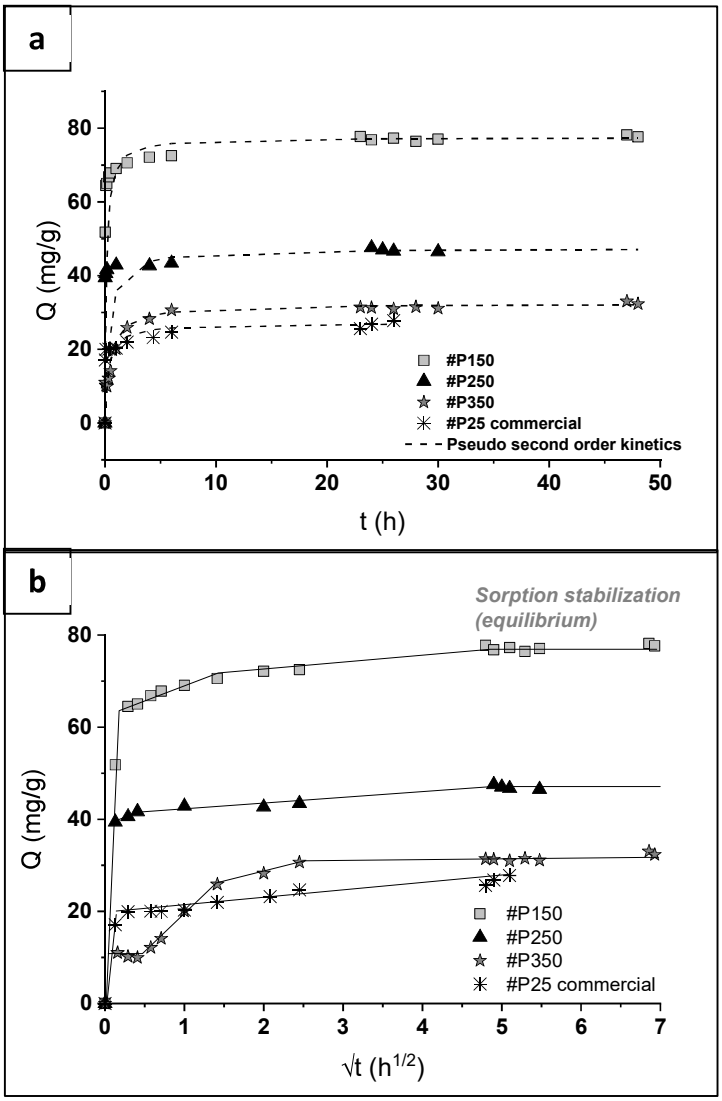

Figure 6 (a) Concentration adsorption isotherms fitted with the Temkin equation, (b) distribution (Kd) isotherms for TiO_2 microspheres prepared in supercritical CO_2 at 150, 250 and 350ºC in suspensions at pH 11